

1 **Continuum Modeling for Neuronal Lamination During Cerebral**
2 **Morphogenesis Considering Cell Migration and Tissue Growth**

3 Hironori Takeda^{a,b}, Yoshitaka Kameo^{a,b,c} and Taiji Adachi^{a,b,c*}

4 *^aDepartment of Micro Engineering, Graduate School of Engineering, Kyoto University,*
5 *Kyoto, Japan; ^bDepartment of Biosystems Science, Institute for Frontier Life and*
6 *Medical Sciences, Kyoto University, Kyoto, Japan; ^cDepartment of Mammalian*
7 *Regulatory Network, Graduate School of Biostudies, Kyoto University, Kyoto, Japan*

8

9 * Corresponding author

10 Taiji Adachi, Ph.D.

11 Laboratory of Biomechanics, Department of Biosystems Science, Institute for Frontier
12 Life and Medical Sciences, Kyoto University

13 53 Shogoin Kawahara-cho, Sakyo, Kyoto, 606-8507, Japan

14 Phone & Fax Number: +81-75-751-4854

15 E-mail: adachi@infront.kyoto-u.ac.jp

16

17

18 **Continuum Modeling for Neuronal Lamination During Cerebral** 19 **Morphogenesis Considering Cell Migration and Tissue Growth**

20 For neuronal lamination during cerebral morphogenesis, later-born neurons must
21 migrate through already-accumulated neurons. This neuronal migration is
22 biochemically regulated by signaling molecules and mechanically affected by
23 tissue deformation. To understand the neuronal lamination mechanisms, we
24 constructed a continuum model of neuronal migration in a growing deformable
25 tissue. We performed numerical analyses considering the migration promotion by
26 signaling molecules and the tissue growth induced by neuron accumulation. The
27 results suggest that promoted migration and the space ensured by tissue growth
28 are essential for neuronal lamination. The proposed model can describe the
29 coupling of mechanical and biochemical mechanisms for neuronal lamination.

30 Keywords: Continuum model; Tissue growth; Cell migration; Cerebral
31 morphogenesis; Neuronal lamination

32

33 **1. Introduction**

34 Cerebral tissue has a well-ordered layered structure consisting of several subtypes of
35 neurons, the formation of which plays an essential role in acquiring physiological brain
36 functions (Rakic 2009). To understand cerebral morphogenesis, it is important to clarify
37 the mechanisms governing the formation of the neuronal layers. Neuronal lamination is
38 accomplished through neuronal migration and accumulation during cerebral
39 morphogenesis. Neurons are produced from radial glial progenitor cells in the
40 ventricular zone (VZ) (Borrell and Reillo 2012; Borrell and Gotz 2014), which is
41 located in the inner region of the cerebrum. The neurons then migrate along the radial

42 glial cells toward the marginal zone (MZ) (Rakic 1972; Borrell and Reillo 2012; Borrell
43 and Gotz 2014), which is located close to the cerebral surface. After reaching the MZ,
44 the neurons stop their migration and accumulate to form an inside-out layered structure
45 in a cortical plate (CP), where the late-born neurons are arranged outside of the early-
46 born neurons (Marin et al. 2010).

47 The neuronal migration during cerebral morphogenesis is regulated by
48 extracellular signaling molecules including reelin (Marin et al. 2010; Valiente and
49 Marin 2010; Chai et al. 2016). Reelin, which is secreted from the neurons in the MZ
50 (D'Arcangelo et al. 1995), is thought to act as a chemoattractant in neuronal migration
51 (D'Arcangelo and Curran 1998; Caffrey et al. 2014). In *reeler* mutants, which have
52 reelin-deficient cerebrums, the neuronal lamination is inverted, forming in an outside-in
53 manner, through inhibition of the neuronal migration (Sheppard and Pearlman 1997).
54 To address the mechanisms governing the formation of inside-out lamination, it is
55 necessary to clarify how neuronal migration is regulated by signaling molecules.

56 To understand neuronal lamination, it is crucial to consider the interaction
57 between cellular and tissue-level mechanisms because the neuronal lamination and
58 tissue formation affect each other. For an example of the tissue formation influencing a
59 cellular-level process, the direction of the neuronal migration can be determined by the
60 orientation of radial glial fibers, which varies depending on the tissue deformation
61 (Misson et al. 1988; Del Toro et al. 2017). In contrast, the volumetric growth in the CP,
62 which is suggested to result in gyrus formation, is caused by the production and
63 accumulation of neurons (Reillo et al. 2011; Borrell and Gotz 2014). This represents an
64 influence of cellular processes on tissue formation. To obtain a conceptual
65 understanding of the cellular and tissue interaction in morphogenesis, computational
66 approaches are useful (Takeda et al. 2020). (#1-1)A variety of computational models of

67 cell dynamics have been proposed in the fields of cell/tissue biology and tissue
68 engineering to study cell movement based on cell-cell adhesion (Armstrong et al. 2006),
69 collective cell migration during wound healing (Buganza Tepole and Kuhl 2016), and
70 scaffold-dependent cell migration (Elsayed et al. 2019). For understanding cerebral
71 development from a biochemical viewpoint, the cellular mechanisms of neuronal
72 lamination, such as the adhesiveness of neurons, have been investigated using
73 computational models (Zubler and Douglas 2009; Caffrey et al. 2014; Matsunaga et al.
74 2017). As for tissue-level mechanisms, computational and theoretical studies have been
75 performed to elucidate the mechanical mechanisms of tissue deformation during
76 cerebral morphogenesis (Budday et al. 2014; Tallinen et al. 2014; Goriely et al. 2015;
77 Tallinen et al. 2016; Rooij and Kuhl 2018). To connect the cellular behavior and tissue
78 deformation, the development of a model coupling neuronal migration and tissue
79 deformation is required.

80 In this study, we constructed a computational model for neuronal lamination
81 caused by neuronal migration in a growing deformable tissue. The tissue growth and
82 deformation were formulated based on continuum mechanics. According to a previous
83 study (Rooij and Kuhl 2018), the cellular migration was described using the balance
84 equation for the cell number density by assuming a constitutive relationship between the
85 cell number density and volumetric growth. To investigate the effects of the promotion
86 of neuronal migration by signaling molecules on the neuronal lamination, the promoted
87 neuronal migration was modeled as an additional migration velocity. Using the
88 proposed model, we performed computer simulations in a one-dimensional space to
89 investigate the effects of the promotion of neuronal migration and tissue growth on the
90 inside-out neuronal lamination.

91

92 2. Continuum model for neuronal lamination in cerebral morphogenesis

93 2.1. Kinematics and constitutive relation of tissue growth

94 We consider a continuum body in a reference configuration, $\mathcal{B}_0 \subset \mathbb{R}^3$, with coordinates
95 \mathbf{X} denoting the position of material points in the body. The position of the same point at
96 time t in the current configuration, $\mathcal{B}_t \subset \mathbb{R}^3$, is denoted as \mathbf{x} . We assume a deformation
97 map, $\chi: \mathcal{B}_0 \rightarrow \mathcal{B}_t$, that maps a material point, \mathbf{X} , in \mathcal{B}_0 to a point $\mathbf{x} = \chi(\mathbf{X}, t)$ in \mathcal{B}_t . The
98 deformation gradient tensor, \mathbf{F} , is defined as $\mathbf{F} := \partial\chi(\mathbf{X}, t)/\partial\mathbf{X}$. To model the material
99 growth, we assume multiplicative decomposition of the deformation gradient tensor, \mathbf{F} ,
100 into a growth part, \mathbf{F}^g , and an elastic deformation part, \mathbf{F}^e , as follows:

$$101 \quad \mathbf{F} = \mathbf{F}^e \mathbf{F}^g. \quad (1)$$

102 The Jacobian of the growth deformation gradient tensor, $J^g := \det \mathbf{F}^g (> 0)$, is
103 the ratio of the volume in the reference configuration to that in the virtual stress-free
104 configuration. To model the cerebral tissue growth induced by the neuronal
105 accumulation, we assume that the volumetric growth depends on the cell number
106 density. With reference to (Rooij and Kuhl 2018), the Jacobian, J^g , is described as a
107 function of the cell number density $c (\geq 0)$ in the current configuration, \mathcal{B}_t :

$$108 \quad J^g(c) = (1 + kc)^\alpha, \quad (2)$$

109 where k and α are parameters for the constitutive relationship between tissue growth
110 and cell number density.

111 2.2. Balance equation for the cell number density

112 The balance equation for the cell number density, c , in the current configuration, \mathcal{B}_t , is
113 given as follows:

$$114 \quad \frac{\partial c}{\partial t} + c \frac{1}{J} \frac{\partial J}{\partial t} = - \frac{\partial}{\partial \mathbf{x}} \cdot \mathbf{q}, \quad (3)$$

115 where $J(> 0)$ is the Jacobian of the deformation gradient tensor, \mathbf{F} , and \mathbf{q} is the flux of
116 the cell number density (Rooij and Kuhl 2018). (#1-2)In this study, cell proliferation and
117 cell death were not included because we focused on the neuronal migration during the
118 lamination. Thus, the source of cell number density was not considered, and the number
119 of cells was constant throughout the simulations. To model the neuronal migration, we
120 describe the flux, \mathbf{q} , as follows:

$$121 \quad \mathbf{q} = c\mathbf{v}\left(1 - \frac{c}{c_{\max}}\right) + c\mathbf{v}_p - D\frac{\partial c}{\partial \mathbf{x}}, \quad (4)$$

122 where \mathbf{v} is the velocity of the neuronal migration, \mathbf{v}_p is the additional velocity of
123 neuronal migration promoted by signaling molecules, c_{\max} is the upper limit of the cell
124 number density when neuronal migration is not promoted, and D is a diffusion
125 coefficient. The first term indicates the flux due to cell density-dependent migration
126 without signaling molecules, and the second term indicates the flux promoted by
127 signaling molecules. (#1-2)The third term indicates the dependence of cell migration on
128 the gradient of cell number density. Substitution of Eq. 4 in Eq. 3 shows that the first
129 and second terms correspond to convection terms, and the third term corresponds to a
130 diffusion term.

131 **2.3. Modeling neuronal lamination**

132 To understand the essential mechanism of the inside-out neuronal lamination, the
133 migration and accumulation of neurons is simulated using a one-dimensional model
134 with a coordinate x (Fig 1). (#2-1-A)Previous studies (D'Arcangelo and Curran 1998;
135 Caffrey et al. 2014) proposed that the inside-out lamination may be achieved through
136 the attractive effect of reelin, which enables the late-born neurons to migrate from the
137 VZ to MZ through the accumulated early-born neurons (Fig. 1, middle panel). The lack

138 of expression of reelin in the *reeler* cerebrum disrupts the neuronal migration, thus
 139 resulting in inverted lamination (Fig. 1, bottom panel).

140 *[Figure 1 near here]*

141 By defining the cell number densities of the early-born and late-born neurons as
 142 c_E and c_L , respectively, the flux of late-born neurons, q_L , in the x -direction can be
 143 described as follows:

$$\begin{aligned}
 q_L &= c_L v \left(1 - \frac{c_E + c_L}{c_{\max}} \right) + c_L v_p - D \frac{\partial c_L}{\partial x} \\
 &= c_L (v + v_p) \left(1 - \frac{c_E + c_L}{(1 + v_p/v) c_{\max}} \right) - D \frac{\partial c_L}{\partial x}, \quad (5)
 \end{aligned}$$

145 where v and v_p are scalar values in the x -direction for the corresponding vector values
 146 in Eq. (4). As shown in Eq. (5), the increase in the additional velocity, v_p , can be
 147 interpreted as an increase in the upper limit of the cell number density. (#2-1-B) In contrast
 148 to the late-born neurons, we assume that the early-born neurons are already accumulated
 149 and do not migrate during the late stage of the lamination, by setting their flux equal to
 150 0.

151 (#2-1-C) To investigate the effects of tissue growth on neuronal lamination at the
 152 late stage, when the accumulated early-born neurons do not contribute to tissue growth,
 153 we considered only the tissue growth caused by the late-born neurons. Using a growth
 154 stretch, θ , in the x -direction determined based on the deformation gradient, \mathbf{F}^g , the
 155 constitutive relationship described in Eq. (2) can be rewritten as follows:

$$\theta = (1 + k c_L)^\alpha. \quad (6)$$

157 The differential equations for tissue growth and neuronal migration were solved
 158 using the finite element method. In the numerical analysis of the tissue growth, the
 159 displacement at $x = 0$ was fixed. For the neuronal migration analysis, Eq. (3) was

160 solved in the one-dimensional domain $0 \leq x \leq l$, where l is the length of the tissue in
161 the current configuration, subject to zero-flux boundary conditions at $x = 0$ and l .

162 3. Results

163 3.1. Neuronal migration through the accumulated neurons

164 (#2-1-D)For inside-out lamination during cerebral morphogenesis, it is essential that late-
165 born neurons migrate through early-born neurons. Based on previous studies proposing
166 the role of reelin as an attractant of neurons (D'Arcangelo and Curran 1998; Caffrey et
167 al. 2014), the effect of reelin was modeled as the promotion of neuronal migration.
168 Using this model, we performed a numerical analysis in a one-dimensional space with
169 coordinate x . In this analysis, the tissue growth was not considered, and thus, the
170 current tissue length, l , was equal to the initial tissue length, L . We considered two types
171 of neurons: the early-born neurons accumulated close to the MZ, and the late-born
172 neurons migrating from the VZ to MZ. At the initial state of the simulations ($t/T = 0$),
173 the cell number density distributions were determined according to an approximated
174 rectangular function. (#2-2)Cell bodies are sparsely distributed behind the accumulated
175 neurons (Sekine et al. 2012; Matsunaga et al. 2017). Thus, the low-density space was
176 set as $0.9 < x/L \leq 1.0$, and the early-born neurons, which had ceased migrating, were
177 set as $0.7 \leq x/L \leq 0.9$ based on cross-sectional images of the cerebrum (Iwashita et al.
178 2014). The late-born neurons, which migrated along the positive x -direction, were set as
179 $0.2 \leq x/L \leq 0.5$. For simplicity, the migration velocity, v , and the additional migration
180 velocity induced by signaling molecules, v_p , in Eq. (5) were assumed to be constant. To
181 investigate the effects of signaling molecules that can promote neuronal migration, the
182 additional velocity, v_p , was set as 0 and $0.2v$. The model parameters were defined as
183 listed in Table 1.

184 *[Table 1 near here]*

185 We investigated the changes in the cell number density distribution with the
186 additional velocity, v_p . When the cell migration was not promoted by signaling
187 molecules ($v_p = 0$), the late-born neurons ceased their migration just before reaching
188 the early-born neurons (Fig. 2A), and thus, the late-born neurons did not migrate
189 through the early-born neurons. On the other hand, in the case where the cell migration
190 was promoted by signaling molecules ($v_p = 0.2v$), the late-born neurons successfully
191 migrated through the early-born neurons (Fig. 2B). These results suggest that the
192 promotion of cell migration by signaling molecules is a possible essential factor for the
193 inside-out lamination in the cerebral cortex.

194 In actual cerebral tissue, the space behind the accumulated neurons is small,
195 and thus we performed numerical simulations by setting two different positions of the
196 accumulated early-born neurons: $0.7 \leq x/L \leq 0.9$ and $0.8 \leq x/L \leq 1.0$. When the
197 space between the early-born neurons and the end of the tissue was smaller, fewer late-
198 born neurons migrated through the early-born neurons (Fig. 2C). On the other hand,
199 when there was no space behind the early-born neurons, the late-born neurons could not
200 migrate through the accumulated early-born neurons; some of the late-born neurons
201 were distributed overlapping with the accumulated neurons, while the rest of the
202 migrating neurons accumulated before the early-born neurons (Fig. 2D). These results
203 suggest that sufficient space is required for all of the cells to migrate through the
204 accumulated cells.

205 ***3.2. Effects of tissue growth on neuronal migration***

206 In the inside-out lamination process, the accumulation of neurons close to the MZ
207 contributes to the volumetric growth of the CP. ^(#2-1-E)In Section 3.1, we found that the
208 low-density space behind the early-born neurons is required for the inside-out

209 lamination. Thus, we consider the expansion of the low-density space through the tissue
210 growth caused by the late-born neurons as a possible mechanism of neuronal lamination.
211 To investigate the effects of the tissue growth on the migration of late-born neurons that
212 pass through the accumulated early-born neurons, we performed numerical simulations
213 of the cell migration in a growing tissue by varying the constitutive parameter k in Eq.
214 (6) (Fig. 3A and 3B). In the initial state of these simulations ($t/T = 0$), the tissue length
215 satisfies $l/L > 1$ as a result of the tissue growth induced by the late-born neurons. The
216 accumulated early-born neurons are present at $l/L - 0.3 \leq x/L \leq l/L - 0.1$, and the
217 late-born neurons are located just before the early-born neurons. In addition to these
218 simulations, to investigate the effects of the space behind the accumulated early-born
219 neurons, we performed simulations by setting the early-born neurons at $l/L - 0.2 \leq$
220 $x/L \leq l/L$ in the initial state (Fig. 3C).

221 *[Figure 3 near here]*

222 Comparing the results for $k = 0.5$ (Fig. 3A) and $k = 1.0$ (Fig. 3B), we show
223 that a larger space behind the early-born neurons enabled a larger number of the late-
224 born neurons to migrate through the accumulated early-born neurons. When there was
225 no space behind the early-born neurons, the late-born neurons could not migrate through
226 the accumulated early-born neurons, even with the growth of the tissue (Fig. 3C). Thus,
227 these results suggest that space behind the accumulated neurons is required for neuronal
228 migration through the accumulated early-born neurons, and this space is ensured by the
229 tissue growth induced by the neuronal accumulation in the MZ.

230

231 **4. Discussion**

232 In cerebral development, neuronal lamination is important for the formation of the
233 functional layered tissue. To investigate the mechanism governing the inside-out
234 neuronal lamination in the cerebral cortex, we simulated the migration of late-born
235 neurons past the accumulated early-born neurons. The simulation results suggest that
236 the neuronal migration must be promoted by signaling molecules to form a neuronal
237 layer behind the accumulated neurons (Fig. 2A and 2B). In addition, a larger number of
238 late-born neurons can pass through the accumulated early-born neurons with increased
239 space behind the accumulated neurons (Fig. 2C and 2D), which suggests that sufficient
240 space behind the accumulated neurons is also required for the formation of inside-out
241 lamination. (#2-1-F)Based on our simulations listed in Section 3.1, we assumed that the
242 low-density space behind the accumulated early-born neurons is expanded by tissue
243 growth induced by the late-born neurons. To test this mechanism, we performed
244 computer simulations considering the tissue growth depending on the cell number
245 density. The results showed that a greater number of late-born neurons can migrate past
246 the accumulated early-born neurons as the tissue grows larger (Fig. 3). Taken together,
247 we have clearly demonstrated that inside-out neuronal lamination can be accomplished
248 through promoted neuronal migration and the tissue growth induced by neuronal
249 accumulation.

250 To investigate the neuronal lamination in cerebral development, it is essential
251 to consider the mechanisms at both the cellular and tissue levels simultaneously. The
252 cellular mechanism of neuronal lamination has been investigated in some previous
253 computational studies (Zubler and Douglas 2009; Caffrey et al. 2014; Matsunaga et al.
254 2017), which focused on biochemical aspects of the cellular interaction, such as the
255 adhesion of neurons. On the other hand, the tissue-level mechanisms of cerebral

256 morphogenesis, such as gyrus formation, have been investigated from a mechanical
257 perspective using mechanical modeling (Budday et al. 2014; Tallinen et al. 2014;
258 Goriely et al. 2015; Tallinen et al. 2016; Rooij and Kuhl 2018). However, the tissue
259 deformation and neuronal lamination processes affect one another, i.e., the neuronal
260 migration depends on tissue deformation (Misson et al. 1988; Del Toro et al. 2017) and
261 tissue growth is caused by neuronal accumulation (Reillo et al. 2011; Borrell and Gotz
262 2014). Therefore, to understand the mechanism of neuronal lamination, it is crucial to
263 investigate the interaction between tissue deformation and neuronal lamination. In this
264 study, we proposed a novel computational model for neuronal lamination and
265 investigated the effects of tissue growth on the neuronal lamination by performing
266 computer simulations of the tissue growth with respect to the cell number density.

267 During neuronal lamination, it has been suggested that reelin secreted from
268 neurons in the MZ plays an important role in regulating neuronal migration.
269 Considering that reelin has been proposed to be a chemoattractive factor during
270 neuronal migration (D'Arcangelo and Curran 1998; Caffrey et al. 2014), in this study,
271 the effect of reelin was modeled as an additional migration velocity. As shown in Eq.
272 (5), this additional velocity corresponds to an increase in the maximum cell number
273 density, which is dependent on cell–cell adhesion. Recent studies have shown that reelin
274 regulates changes in the adhesiveness of neurons (Sekine et al. 2012; Matsunaga et al.
275 2017). Therefore, the simulation results shown in Fig. 2 suggest that reelin enables the
276 late-born neurons to migrate past the early-born neurons by enhancing the velocity of
277 the neuronal migration or by inducing a decrease in the cell–cell adhesion, which results
278 in an increase in the maximum cell number density. Additionally, reelin has been
279 suggested to regulate formation of the MZ, in which cell bodies are sparsely distributed
280 (Sekine et al. 2012; Matsunaga et al. 2017). Therefore, our simulation results suggest

281 that reelin also contributes to the inside-out lamination by creating the space behind the
282 accumulated early-born neurons by decreasing the cell density in the MZ.

283 (#2-3, #2-4, #2-5) We performed numerical analyses in a one-dimensional space
284 because the inside-out lamination is essentially one-dimensional. To investigate the
285 mechanical effects of tissue deformation on the neuronal lamination, such as tissue
286 folding during gyrus formation, two- or three-dimensional analysis must be performed.
287 This analysis could also consider both radial migration and non-radial/tangential
288 migration, such as locomotion in CP, terminal translocation in MZ, and multipolar
289 migration in VZ. Although such modes of neuronal migration contribute to the
290 formation of neuronal layers, we modeled only locomotion of neurons in this study. To
291 model the different migration modes, it is important to consider the heterogeneity of
292 direction and speed of neuronal migration depending on the migration mode. These
293 types of models would enable us to investigate the duration of neuronal lamination and
294 the distribution of region-dependent thickness of neuronal layers. Furthermore, in
295 addition to neuronal migration, modeling of the subsequent neuronal behaviors, such as
296 cell fate decisions and maturation of neurons, will contribute to a comprehensive
297 understanding of cerebral morphogenesis.

298 This study developed a computational model for neuronal lamination in
299 growing tissue based on a continuum model. To understand the essential mechanism
300 governing the neuronal lamination, we performed numerical analyses in a one-
301 dimensional space by focusing on the locomotion of neurons. Further development of
302 this model can lead to the establishment of a computational platform to understand the
303 mechanisms governing the formation of functional tissues.

304

305

306 **Acknowledgments**

307 This work was supported by JSPS KAKENHI Grant Number JP16H06486 and by a
308 Grant-in-Aid for JSPS fellows (19J14843) from JSPS.

309

310 **Declaration of Interest**

311 There are no conflicts of interest to declare.

312

313 **References**

- 314 Armstrong NJ, Painter KJ, Sherratt JA. 2006. A continuum approach to modelling cell-
315 cell adhesion. *J Theor Biol.* 243(1):98-113.
- 316 Borrell V, Gotz M. 2014. Role of radial glial cells in cerebral cortex folding. *Curr Opin*
317 *Neurobiol.* 27:39-46.
- 318 Borrell V, Reillo I. 2012. Emerging roles of neural stem cells in cerebral cortex
319 development and evolution. *Dev Neurobiol.* 72(7):955-971.
- 320 Budday S, Raybaud C, Kuhl E. 2014. A mechanical model predicts morphological
321 abnormalities in the developing human brain. *Sci Rep.* 4:5644.
- 322 Buganza Tepole A, Kuhl E. 2016. Computational modeling of chemo-bio-mechanical
323 coupling: a systems-biology approach toward wound healing. *Comput Methods*
324 *Biomech Biomed Engin.* 19(1):13-30.
- 325 Caffrey JR, Hughes BD, Britto JM, Landman KA. 2014. An in silico agent-based model
326 demonstrates Reelin function in directing lamination of neurons during cortical
327 development. *PLoS One.* 9(10):e110415.
- 328 Chai X, Zhao S, Fan L, Zhang W, Lu X, Shao H, Wang S, Song L, Failla AV, Zobiak B
329 et al. 2016. Reelin and cofilin cooperate during the migration of cortical neurons: a
330 quantitative morphological analysis. *Development.* 143(6):1029-1040.
- 331 D'Arcangelo G, Curran T. 1998. Reeler: new tales on an old mutant mouse. *Bioessays.*
332 20(3):235-244. eng.
- 333 D'Arcangelo G, Miao GG, Chen SC, Soares HD, Morgan JI, Curran T. 1995. A protein
334 related to extracellular matrix proteins deleted in the mouse mutant reeler. *Nature.*
335 374(6524):719-723.
- 336 Del Toro D, Ruff T, Cederfjall E, Villalba A, Seyit-Bremer G, Borrell V, Klein R. 2017.
337 Regulation of Cerebral Cortex Folding by Controlling Neuronal Migration via FLRT
338 Adhesion Molecules. *Cell.* 169(4):621-635 e616.
- 339 Elsayed Y, Lekakou C, Tomlins P. 2019. Modeling, simulations, and optimization of
340 smooth muscle cell tissue engineering for the production of vascular grafts. *Biotechnol*
341 *Bioeng.* 116(6):1509-1522.

342 Goriely A, Budday S, Kuhl E. 2015. Chapter 2, Neuromechanics: From Neurons to
343 Brain. In: Bordas SPA, Balint DS, editors. *Advances in Applied Mechanics*. Elsevier; p.
344 79-139.

345 Iwashita M, Kataoka N, Toida K, Kosodo Y. 2014. Systematic profiling of
346 spatiotemporal tissue and cellular stiffness in the developing brain. *Development*.
347 141(19):3793-3798.

348 Marin O, Valiente M, Ge X, Tsai LH. 2010. Guiding neuronal cell migrations. *Cold*
349 *Spring Harb Perspect Biol*. 2(2):a001834.

350 Matsunaga Y, Noda M, Murakawa H, Hayashi K, Nagasaka A, Inoue S, Miyata T,
351 Miura T, Kubo KI, Nakajima K. 2017. Reelin transiently promotes N-cadherin-
352 dependent neuronal adhesion during mouse cortical development. *Proc Natl Acad Sci U*
353 *S A*. 114(8):2048-2053.

354 Misson J-P, Edwards MA, Yamamoto M, Caviness VS. 1988. Identification of radial
355 glial cells within the developing murine central nervous system: studies based upon a
356 new immunohistochemical marker. *Dev Brain Res*. 44(1):95-108.

357 Rakic P. 1972. Mode of cell migration to the superficial layers of fetal monkey
358 neocortex. *J Comp Neurol*. 145(1):61-83. eng.

359 Rakic P. 2009. Evolution of the neocortex: a perspective from developmental biology.
360 *Nat Rev Neurosci*. 10(10):724-735.

361 Reillo I, de Juan Romero C, Garcia-Cabezas MA, Borrell V. 2011. A role for
362 intermediate radial glia in the tangential expansion of the mammalian cerebral cortex.
363 *Cereb Cortex*. 21(7):1674-1694.

364 Rooij Rd, Kuhl E. 2018. A physical multifield model predicts the development of
365 volume and structure in the human brain. *J Mech Phys Solids*. 112:563-576.

366 Sekine K, Kawauchi T, Kubo K, Honda T, Herz J, Hattori M, Kinashi T, Nakajima K.
367 2012. Reelin controls neuronal positioning by promoting cell-matrix adhesion via
368 inside-out activation of integrin $\alpha 5\beta 1$. *Neuron*. 76(2):353-369.

369 Sheppard AM, Pearlman AL. 1997. Abnormal reorganization of preplate neurons and
370 their associated extracellular matrix: an early manifestation of altered neocortical
371 development in the reeler mutant mouse. *J Comp Neurol*. 378(2):173-179. eng.

372 Takeda H, Kameo Y, Inoue Y, Adachi T. 2020. An energy landscape approach to
373 understanding variety and robustness in tissue morphogenesis. *Biomech Model*
374 *Mechanobiol.* 19(2):471-479.

375 Tallinen T, Chung JY, Biggins JS, Mahadevan L. 2014. Gyrification from constrained
376 cortical expansion. *P Natl Acad Sci USA.* 111(35):12667-12672.

377 Tallinen T, Chung JY, Rousseau F, Girard N, Lefèvre J, Mahadevan L. 2016. On the
378 growth and form of cortical convolutions. *Nat Phys.* 12(6):588-593.

379 Valiente M, Marin O. 2010. Neuronal migration mechanisms in development and
380 disease. *Curr Opin Neurobiol.* 20(1):68-78.

381 Zubler F, Douglas R. 2009. A framework for modeling the growth and development of
382 neurons and networks. *Front Comput Neurosci.* 3:25.

383

384

385 **Tables**

386 Table 1. Model parameters

Symbol	Value	Descriptions
L	100 μm	Initial length of the tissue
T	1 day	Representative time of the neuronal lamination
v	500 $\mu\text{m}/\text{day}$	Velocity of the neuronal migration in Eq. (5)
D	500 $\mu\text{m}^2/\text{day}$	Diffusion coefficient in Eq. (5)
c_{max}	1 / μm	Upper limit of the cell number density in Eq. (5)
α	1	Constitutive parameter in Eq. (6)

387

388 **Figure captions**

389 Figure 1. One-dimensional model of the neuronal lamination. Neurons born from radial
390 glial progenitor cells (black) in the VZ migrate toward the MZ; after reaching the MZ,
391 the neurons stop their migration and accumulate in a CP (top panel). The neuronal
392 lamination proceeds in an inside-out manner, in which the late-born neurons (red)
393 migrate past the accumulated early-born neurons (blue) (middle panel). The lack of
394 expression of reelin in the *reeler* cerebrum disrupts the neuronal migration, thus
395 resulting in inverted lamination (bottom panel).

396

397 Figure 2. Numerical analysis of neuronal lamination in one-dimensional space. The
398 curves show the spatial distributions of the early born neurons (blue) and the late-born
399 neurons (warm colors) at time t . The late-born neurons migrate toward the accumulated
400 early-born neurons along the positive x -direction. **(A)** Neuronal migration when the
401 migration was not promoted by signaling molecules ($v_p = 0$). **(B)** Neuronal migration
402 past the accumulated neurons when the migration was promoted by signaling molecules
403 ($v_p = 0.2v$). **(C, D)** Effects of the space between the early-born neurons and the end of
404 the tissue on neuronal lamination. **(C)** Neuronal migration with a smaller space behind
405 the accumulated neurons than that in **(B)**. **(D)** Neuronal migration with no space behind
406 the early-born neurons.

407

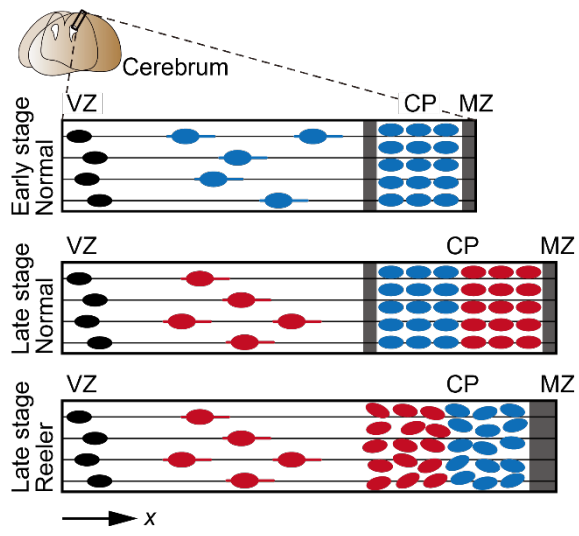
408 Figure 3. Effects of tissue growth on neuronal lamination. The snapshots show the
409 spatial distribution of the cell number density for the late-born neurons (red) and early-
410 born neurons (blue) at the varying times, t . **(A, B)** Migration of the late-born neurons
411 through the accumulated early-born neurons with varying constitutive parameter of
412 tissue growth, k , in Eq. (6): **(A)** $k = 0.5$ and **(B)** $k = 1.0$. The dotted lines represent

413 growth stretch, θ . The gray regions indicate the outside of the tissue. (C) Neuronal
414 migration with the tissue growth ($k = 1.0$) when there is no space behind the
415 accumulated early-born neurons.

416

417 **Figures**

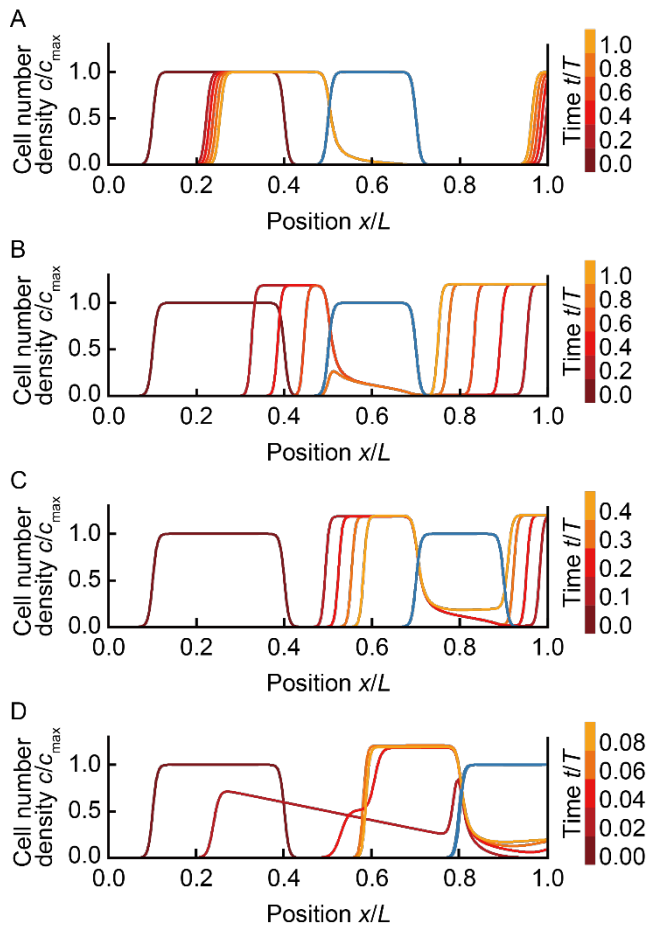
418



419

420 **Figure 1**

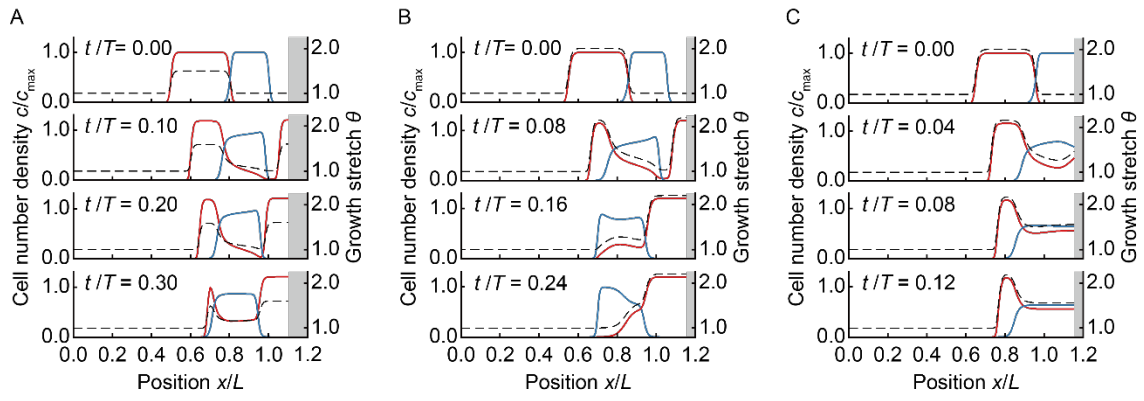
421



422

423 Figure 2

424



425

426 Figure 3